

Effect of SiO₂ dispersion on chlorine-induced high temperature corrosion of HVAF-sprayed NiCrMo coating

Esmaeil Sadeghimeresht^{a1}, Nicolaie Markocsan^a, Tanvir Hussain^b, Matti Huhtakangas^c, Shrikant Joshi^a

^a Department of Engineering Science, University West, 461 53 Trollhättan, Sweden

^b Faculty of Engineering, The University of Nottingham, Nottingham NG7 2RD, UK

^c M. H. Engineering AB, 691 42 Karlskoga, Sweden

Abstract

NiCrMo coatings with and without dispersed SiO₂ were deposited using high velocity air-fuel (HVAF) technique. Thermogravimetric experiments were conducted in 5% O₂+500 vppm HCl+N₂ with and without a KCl deposit at 600 °C for up to 168 h. The SiO₂-containing coating showed lower weight change due to formation of a protective and adherent Cr-rich oxide scale. SiO₂ decelerated short-circuit diffusion of Cr³⁺ through scale's defects, e.g., vacancies, and promoted the selective oxidation of Cr to form the protective Cr-rich oxide scale. Furthermore, the presence of SiO₂ led to less subsurface depletion of Cr in the coating, and accordingly less corrosion of the substrate. The formed corrosion product on the SiO₂-free coating was highly porous, non-adherent, and thick.

Keywords: Thermal Spray Coating; Chlorine-Induced High Temperature Corrosion; NiCrMo; SiO₂ Dispersion; High Velocity Air-Fuel (HVAF); Biomass-/Waste-Fired Boiler

¹ Corresponding author: E-mail address: esmaeil.sadeghimeresht@hv.se (E. Sadeghimeresht)

1 Introduction

Demands for increasing the lifetime of components and thermal/electrical efficiency in power generation industry, particularly in biomass- and waste-fired boilers, are incessantly growing [1]–[3]. For this reason, application of appropriate coatings with longer endurance in the highly corrosive service environments routinely encountered in boilers is imperative [4]–[7]. Thermally sprayed metallic coatings have frequently been employed to enhance the corrosion resistance of boiler's components [8]–[12]. In this context, obtaining a dense and adherent thermal spray coating that is maintenance free for an extended period of time is always desirable and provides motivation for further investigation of promising coating materials and processes [13], [14].

There have been several efforts to enhance the corrosion resistance of thermal spray coatings by studying different a) coating compositions, using various feedstock material chemistries [15] and b) coating microstructures, using appropriate thermal spray process parameters or post-spray treatments [16], [17]. Another potential approach is to alter the coating architecture either by creating a new coating design, such as multilayered or functionally graded coatings [18], or by incorporating certain oxygen-active elements (like SiO_2 , Al_2O_3 or Y_2O_3) into the coating to fabricate composite structures [19], [20]. It has already been reported that the high-temperature corrosion performance of alloys can be improved by uniformly distributed oxide dispersoids, which act as nucleation sites and facilitate eventual formation of a continuous, dense and protective oxide scale on the surface [21]. However, this proposed mechanism is under debate and has been rejected by others [22], as no change can be seen between the oxidation behavior of a dispersoids-containing alloy and a free-dispersoids alloy at the early stages of oxidation exposure. Therefore, it is proposed that the dispersoids alter microstructure of the formed oxide by reducing the grain size which promotes inward diffusion of O^{2-} rather than outward diffusion of Cr^{3+} through the oxide grain boundaries [22]. The dispersed oxides can lead to excellent scale adherence to the substrate material based on a mechanism known as “pegging effect” or “mechanical keying”, as frequently reported by various authors [23], [24]. The oxide scale protrusions into the underlying alloy was also found which pin the scale to the substrate. The dispersed oxides in the alloy are also reported to act as preferred sites for nucleation of vacancies which are, therefore, prevented from concentrating at the oxide scale/metal interface [25].

Thermal spray processes can be used to deposit such composite coatings comprising dispersed oxides. However, there are a few technical drawbacks with the commonly used thermal spray techniques, e.g., high velocity oxy-fuel (HVOF) and atmospheric plasma spraying (APS) to spray such coatings [19], [23]. As the dispersed oxides are usually very fine ($< 1\ \mu\text{m}$), they can decompose at very high processing temperatures. Such fine oxides also need to be dispersed uniformly within the coating rather than being agglomerated locally. High velocity air-fuel (HVOF) technique is proposed to overcome such drawbacks as the process benefits from the lowest temperature ($T < 1800\ ^\circ\text{C}$), and highest velocity ($V = 700\text{--}1500\ \text{m/s}$) of the flame compared to other thermal spray processes like plasma spray and HVOF.

By virtue of these, dense and adherent coatings with least *in-situ* phase decomposition/oxidation can be produced which are greatly desired in corrosion protection applications [26].

Limited number of studies have focused on the high temperature corrosion resistance of dispersed oxide-containing alloys in oxidizing and chloridizing-oxidizing environments. Even less information is available regarding thermally sprayed coatings containing dispersoids. More specifically, to the best of the authors' knowledge, no publication is available regarding Cl-induced high temperature corrosion behaviour of HVAF-sprayed Ni-based coatings containing dispersoids. The diffusion mechanisms of Cl and O through the oxide scale and interaction with the complex chemistry of coatings with dispersed oxides are still unknown. Understanding corrosion mechanisms in coatings is of crucial significance as it can assist in charting pathways to mitigate the rate of degradation and thereby assist in the development of advanced coatings that can potentially be highly protective even in harsh working environments.

Therefore, the aim of the present work was to investigate the potential implication of a dispersed oxide, i.e., SiO₂ in NiCrMo coatings sprayed using HVAF on the Cl-induced high temperature corrosion behavior. Understanding the different transport phenomena in the oxide scale and the differences in scale morphology of the coatings with and without SiO₂ dispersion will be highly educative. Based on the observations, possible mechanisms of scale formation and growth have been discussed herein.

2 Experimental procedures

2.1.1 Feedstock powders

A gas-atomized powder of Ni₂₁Cr₉Mo (with a nominal composition of 20.2 Cr-7.9Mo-0.1O-Ni bal. all in wt%) sourced from H.C. Starck GmbH (Germany) (referred to as NiCrMo hereafter) and a proprietary SiO₂-containing Ni₂₁Cr₉Mo powder supplied by M.H. Engineering AB (Sweden) (referred to as NiCrMo-SiO₂ hereafter) were used to produce the coatings. The particle size of the feedstock powders was -45 +15 μm and -45+22 μm for NiCrMo and NiCrMo-SiO₂, respectively. Fig. 1 shows the spherical morphology, and dendritic structure of the two powders resulted from the segregation of heavy elements like Mo during the gas atomization process. Very few satellite particles around large particles which are also typically found in morphology of gas-atomized powders [27] can be seen in the figure.

2.1.2 Substrate material

Rods of a commercial low carbon steel 16Mo3 (nominal composition in wt%; 0.01Cr- 0.3Mo- 0.5 Mn- 0.3Si- 0.15C- Fe bal.) of 160 mm diameter and 500 length were used as substrate. All specimens were grit blasted with alumina particles (-63+10 μm) for cleaning and roughening prior to spraying.

2.2 HVAF spraying

A M3TM-HVOF spraying system (Uniquecoat, Oilville, VA, USA) was employed to deposit the coatings. A horizontal rotating fixture was used to grip the 16Mo3 rod in order to first coat on its cylindrical surface. The rod was then cut into buttons of 5 mm thickness. Both flat surfaces of the buttons were then HVOF sprayed, so that the specimens were fully coated (on all sides). More details about the substrate preparation can be found in a previous work [28].

4L2G was used as a secondary nozzle in the HVOF process. The pressure of compressed air was set to ~ 0.8MPa, whereas the pressures of fuel 1 (propane) and fuel 2 (propane) were kept similar at ~ 0.7MPa. The powder carrier gas was N₂ with a pressure of ~ 0.4MPa. The powder feed rate was ~ 150 g/min. The pass velocity and pass spacing of the HVOF gun were 50 m/min and 5 mm/rev., respectively. The spray distance (SoD) was 300 mm and eight passes were implemented to achieve the desired coating thickness of ~ 250 µm. These final process parameters were selected based on preliminary coating trials conducted to obtain the least porous microstructure [29]. Prior to the corrosion test, all surfaces of the investigated samples were polished with a 0.05 µm colloidal alumina suspension to a roughness of $R_a < 0.1$ µm in order to get a uniform surface roughness on all coatings.

2.3 Chlorine-induced corrosion test

The corrosion tests were conducted in 5 vol.%O₂ + 500 vppm HCl + N₂ up to 168h at 600 ± 1 °C with and without KCl salt deposit using individual alumina crucibles in a horizontal alumina tube furnace. A KCl suspension was prepared with ethanol and distilled water (with the mix ratio of 4 to 1, respectively). The KCl salt was deposited on the samples (~ 0.1 mg/cm²) using a paintbrush. A mass flow controller was used to introduce 35 cm³/min of gas through the chamber during the high-temperature corrosion test. More details about the furnace can be found in [30]. The samples were under the flow of N₂ throughout the course of exposure to prevent corrosion during cooling. Just before the test, both samples and crucibles were individually weighed using a LE26P Poly Range Microbalance (SartoriusTM, Massachusetts, USA). The crucible and sample with KCl were also weighed to calculate the amount of KCl placed on the surface of the sample. The samples were extracted from the furnace after the test and weighed in their individual crucibles together with the oxide scale spalled from the exposed coatings.

The growth rate of uniform and dense oxide scales is commonly assumed to be controlled by diffusion of elements through the scales [31]. A simplified analysis of this situation is carried out to show that rate control by such a process leads to the parabolic kinetics according to Eq. 1:

$$\left(\frac{\Delta w}{A}\right)^2 = k_p \cdot t \quad (1)$$

where Δw = the weight gain per unit area A (mg/cm²), t = the oxidation time in s, and k_p = the parabolic rate constant for scaling weight gain at each temperature.

2.4 Characterization of coatings

2.4.1 Scanning Electron Microscopy (SEM) and Energy-Dispersive X-ray (EDS)

The cross-section of the as-sprayed and exposed coatings was investigated using a QUANTA-200 FEG scanning electron microscope (FEI, Oregon, USA) equipped with X-ray energy dispersive spectroscope (EDS). For the topographical investigation, the SE (secondary electron) detector with 15 kV and for the cross sectional studies, BSE (backscattered electron) detector with 20 kV were used. To analyze the cross sections, the as-sprayed coatings were cut slowly (with a disk speed of 300 rpm and feed rate of 0.005 mm/min) using a diamond-tipped precision circular saw and then cold mounted in a low shrinkage resin to prevent spallation of the formed oxide scale. The mounted samples were ground/polished to a 0.05 μm colloidal alumina finish.

2.4.2 Porosity measurement

ImageJ (NIH, USA) software, an image analysis (IA) technique, was utilized to determine the extent of porosity in coatings [32] by converting the SEM micrographs of the cross-section (with horizontal field width of 100 μm) into binary images, and quantifying the percentages based on the grey scale contrast [33]. The amount of porosity measured on ten different SEM images were averaged and reported per sample.

2.4.3 X-ray Diffraction (XRD)

A D5000 X-ray diffractometer (Siemens, Germany), equipped for grazing incidence analysis with Cr- K_{α} radiation ($\lambda=0.229\text{ nm}$) operating with a fixed incident angle of 1° and diffraction angle (2θ) between 25° and 80° , was used to identify the phases present in the coating and in the corrosion products after exposure. The analysis of the diffractograms was performed with DIFFRAC.EVA using the ICDD-PDF database for phase identification.

2.4.4 Surface roughness

A stylus-based profilometer (Surftest 301, Mitutoyo, Japan) was used to measure the surface roughness (R_a) of the coatings. The reported values were the average of ten measurements.

3 Results and discussion

3.1 Surface morphology, cross section, and XRD analysis of as-sprayed coatings

Fig. 2 (a-b) presents the SEM surface topography of the as-sprayed NiCrMo and NiCrMo-SiO₂ coatings revealing similar morphologies, i.e., a semi-molten characteristic with unmelted particles evident on the top surface. This may be a consequence of the low temperature of the HVOF process leading to formation of semi-melted particles, some of which do not plastically deform and entirely flatten over the surface [34]. Lack of peening effect is known to cause the formation of such features on the surface of HVOF coatings [35]. The rather wide distribution in particle size ($-45+22\text{ }\mu\text{m}$ for NiCrMo-SiO₂, and

-45+15 μm for NiCrMo) is also a contributing factor, as the coarse particles present in the feedstock have a relatively greater tendency to remain unflattened.

The as-sprayed surface roughness (R_a) of the NiCrMo and NiCrMo-SiO₂ coatings was measured as 8.1 ± 1.1 and 6.9 ± 0.8 μm , respectively; however, both coatings were ground/polished (to $R_a < 0.1$ μm) before the high temperature exposures in order to unify the effect of surface roughness on the corrosion resistance. The EDS analysis in point A (Fig. 2a) showed that the surface composition of the NiCrMo coating was (all in wt%) 20.9Cr-8.3Mo-0.6O-bal. Ni, whereas it was 22.5Cr-8.3Mo-4.5Si-2.9O-bal. Ni for NiCrMo-SiO₂ in point B (Fig. 2b), indicating that Si, most probably in form of SiO₂, was incorporated into the latter coating.

Fig. 3(a-b) shows the cross-sections of the as-sprayed NiCrMo and NiCrMo-SiO₂ coatings. A few unmelted particles were seen in NiCrMo. The emergence of such unmelted particles can be attributed to the presence of particles of various sizes in the feedstock powder, which are heated up, softened, and eventually melted to varying extent during spraying. This can also be due to the typically short dwell time of *in-flight* particles and low temperature in the HVOF jet stream [36]. Usually, the coarse particles are not completely melted in the flame and/or fully flattened upon impingement, resulting in a gap or pore being formed between the splats. NiCrMo-SiO₂ in Fig. 3(b) presented a much denser microstructure

The splat boundaries in NiCrMo-SiO₂ were concealed even at very high magnification (see Fig. 3b), whereas the splat boundaries in NiCrMo (Fig. 3a) can be clearly observed. Although the content of porosity was relatively higher in NiCrMo (1.3 ± 0.3 vol.%) than NiCrMo-SiO₂ (0.9 ± 0.2 vol.%), the values in both coatings suggested that they can be potentially promising for being used in corrosion protection applications. The EDS analysis in the cross sections of the two coatings (points A and B similarly taken from the surrounding of splashed particles in Fig. 3) also confirmed the relatively low level of oxygen pick up during spraying. Such low levels of porosity, low oxygen pick up during coating and high adherence of the coating to substrate can exclusively be attributed to the high velocity and low temperature of the *in-flight* particles in HVOF [30]. A higher level of oxygen detected in NiCrMo-SiO₂ was due to the presence of the oxygen-containing dispersoid (SiO₂) in the coating.

According to the XRD patterns presented in Fig. 4, the NiCrMo powder displayed only γ -Ni (FCC solid solution crystal structure) with no other phases present. NiCrMo-SiO₂ presented primary peaks of γ -Ni as well as SiO₂. The powders showed much sharper X-ray diffraction peaks than that of the as-sprayed coatings. Broadening of the XRD peaks in case of the coatings occurred because of the considerable decrease in crystallite size and increased lattice strain resulting from plastic deformation during HVOF spraying [36]. The XRD patterns of the coatings (Fig. 4) showed that the Ni peaks slightly shifted towards higher 2θ angles which might be due to the increased level of residual stresses within the coatings [37] after spraying. The XRD results proved that the HVOF process did not affect the phase composition of the feedstock powders, by either forming new phases or altering the pre-existing phases. The SiO₂ phase present in NiCrMo-SiO₂ coating is a consequence of the composition of the proprietary

powder feedstock, and specifically intended to modify the oxidation mechanism of the sprayed coating, with the SiO_2 plausibly promoting the selective oxidation of Cr to form the protective Cr-rich oxide layer on the surface [38] as discussed in the subsequent sections. Further analysis of the diffraction patterns showed that SiO_2 were present in different crystalline forms in the NiCrMo- SiO_2 coating including cristobalite, quartz, and coesite. Although such crystalline forms attain different physical characteristics due to their internal structures (owing to different arrangements of Si and O layers), the chemical composition is identical (each Si is always surrounded by four O atoms). Moreover, as these crystalline forms of SiO_2 are stable in the high temperature corrosion test condition of the present study (600 °C) [39], these three phases were similarly considered as SiO_2 . The effect of each SiO_2 crystalline phase on the high temperature corrosion behavior of the coatings is not under the scope of the present study, but a research subject for further investigation in future.

3.2 Weight change in coatings after high temperature corrosion exposure

Fig. 5 shows the weight change of the NiCrMo and NiCrMo- SiO_2 coatings subjected to corrosion in 5% O_2 +500 vppm HCl+N₂ at 600 °C with and without KCl at various time intervals up to 168 h. It is pertinent to mention that the weight change for the coated samples can be sourced from different factors as follows;

- a) Formation of oxides such as Cr_2O_3 or NiCr_2O_4 [28],
- b) Formation of metallic chlorides, mainly NiCl_2 , MoCl_3 , CrCl_3 , or CrCl_2 within the coating [40],
- c) Evaporation of metallic chlorides, e.g., NiCl_2 , MoCl_3 , or/and CrCl_2 which can possibly form in such Cl-containing environment [41].
- d) Spallation of corrosion products [42],
- e) Deterioration of the substrate (16Mo3) by Cl and formation of new phases (either oxides or chlorides) at the coating/substrate interface [30], and
- f) Sintering of KCl on the surface during the exposure [43],

while the problem with the spallation was coped using the crucibles to collect corrosion products in case of possible spallation, the total weight change reported for each time step in Fig. 5 was a combination of the above sources. Once a weight gain was recorded, it implied that the factors leading to weight gain (such as formation of an oxide) outweighed the factors leading to weight loss (such as vaporization) and vice versa. Such considerations were further investigated in the following sections. Considering the potential sources in the weight change, the recorded weight change of the coatings exposed to KCl was much higher than that of the coatings exposed without KCl. Moreover, without KCl, the weight change of NiCrMo- SiO_2 was slightly lower than that of NiCrMo, whereas the weight change of NiCrMo- SiO_2 was much lower than NiCrMo when KCl was introduced. The lower weight change of NiCrMo- SiO_2 exposed to O_2 +HCl with KCl at all exposure times indicated that SiO_2 played a major contributory role in ensuring that the coating was more protective in corrosion protection in harsh corrosion environment. Thirdly, a significant drop in the weight change of NiCrMo from 96 h to

168 h exposure can be seen, whereas no such drop was observed in the weight change of NiCrMo-SiO₂. The rate of weight gain was rapid during early stages of the exposure implying that the elements present in the coatings, e.g., Ni, Cr, and Mo, reacted with O (available in the environment) to form the corresponding oxides. The important determining factors from a protection standpoint are how fast a continuous, stable, and protective scale develops on the coatings, how long such a scale can last and how regeneration/replacement of the scale occurs. Once KCl is introduced, there can be a competition between O and Cl to form the oxides and volatile metallic chlorides. During the late stages of exposure, formation of the volatile metallic chlorides on NiCrMo plausibly outweighed the formation of oxides resulting in a drop in weight, whereas in the early stages oxide formation led to weight gain [30]. It can be assumed that the oxide formed on the SiO₂-free NiCrMo coating exposed to O₂+HCl with KCl was not dense and protective enough which needs to be confirmed by SEM/EDS analysis. Therefore, the inward diffusion of oxygen continued and enhanced the internal oxidation of the coatings. In the NiCrMo-SiO₂ coating, the rate of weight change was rather slow in comparison. It can be assumed that, in this coating, the finely distributed dispersoids of SiO₂ in the coating most probably promoted the selective oxidation of Cr to form Cr₂O₃ nuclei initially on the surface of the coating exposed to the corrosive environment, leading to the eventual formation of a continuous and protective oxide scale [44]. This will be further discussed in the following sections.

It is pertinent to mention that the weight change data reported above were for the polished coatings. It was shown that the surface roughness has a substantial contribution to the weight change of the coatings [34]. The impact of surface roughness on the high temperature corrosion behavior was studied in a previous work [34]. The previous work performed in an ambient air environment at 600 °C for 168 h indicated that reducing the surface roughness to $R_a < 0.1 \mu\text{m}$ resulted in the weight gain of the NiCrMo-SiO₂ coating being reduced by ~71% compared to the non-polished coating. Such behavior could be attributed to either the higher level of residual stresses (above the roughness peaks) which lead to oxide spallation/cracking, or higher surface area exposed to the environment in the as-sprayed coatings [45]. Fig. 5b shows the obtained data of squared weight gain in a plot of $(\Delta w/A)^2$ as a function of (t in sec.) according to Eq. (1) to obtain the values of k_p . The lowest k_p value was measured for NiCrMo-SiO₂ exposed without KCl ($\sim 1.6 \times 10^{-7} \text{ mg}^2/\text{cm}^4\text{s}$) followed by NiCrMo exposed without KCl ($\sim 3.3 \times 10^{-7} \text{ mg}^2/\text{cm}^4\text{s}$). The highest k_p value was calculated as $\sim 7.9 \times 10^{-5} \text{ mg}^2/\text{cm}^4\text{s}$ for NiCrMo exposed with KCl. The calculated parabolic rate constants of the NiCrMo-SiO₂ and NiCrMo coatings exposed without KCl fell within the range of $3.3 \times 10^{-9} - 2.8 \times 10^{-7} \text{ mg}^2/\text{cm}^4\text{s}$, typically reported for chromia-forming bulk materials [46], [47]. However, the k_p values were much higher once KCl was introduced to the environment implying that the aggressive environment facilitated formation of other corrosion products rather than chromia. It should be also noted that the parabolic rate for Cr₂O₃ scale growth may vary depending on temperature and composition.

3.3 Composition and morphology of corrosion products

Fig. 6 shows the XRD patterns of the corrosion products formed on the NiCrMo and NiCrMo-SiO₂ coatings after exposure at 600 °C for 168 h. The corrosion product formed on the NiCrMo coating exposed to O₂+HCl without KCl was mainly composed of NiCr₂O₄ and MoO₃, whereas the scale observed on NiCrMo-SiO₂ coating consisted of mainly Cr₂O₃ and SiO₂. The latter corrosion product had probably a very low thickness since the signal from the background (γ -Ni in the as-sprayed coating) was also identified as confirmed by subsequent SEM visualization of the cross-sections of the exposed coatings. When KCl was introduced, NiCr₂O₄, MoO₃, and CrCl₃ were formed on NiCrMo. However, no sign of CrCl₃ was identified on NiCrMo-SiO₂, although NiCr₂O₄, SiO₂, and Cr₂O₃ were observed. Lack of K₂CrO₄ in the XRD patterns of both coatings was probably due to low penetration depth of X-ray.

The topographic micrographs of the coatings exposed to O₂+HCl with KCl are shown in Fig. 7 (a-b). While formation of detrimental K₂CrO₄ was not observed in XRD, this oxide can be seen in Fig. 7a along with wrinkled Cr₂O₃ according to their topographical features reported in the literature [30], [48]. Formation of such phases need to be further analyzed by SEM/EDS of the cross-sections of the exposed coatings, which is discussed in the next sections. While SiO₂ mostly covered the surface of the NiCrMo-SiO₂ coating, sintered KCl can also be seen, confirming that the environment remained oxidizing-chloridizing during the course of exposure.

3.4 Structure and surface morphology of corrosion products

The cross-section of the coatings exposed to O₂+HCl with and without KCl at 600 °C after 168 h of exposure is shown in Fig. 8. It was found that both the NiCrMo and NiCrMo-SiO₂ coatings exposed in the absence of KCl (Fig. 8a-b) retained their protective oxide scales (a thin layer of chromia detected by XRD in Fig. 6) without any detectable Cr-depletion zone. The integrity of the coatings to substrates were also confirmed as no sign of new phases were observed at the coating/substrate interfaces. When KCl was introduced, a thick, non-adherent, and porous layer of corrosion products formed on NiCrMo whereas the layer of corrosion products formed on NiCrMo-SiO₂ was rather dense and adherent. The NiCrMo-SiO₂ coating was still adherent to the substrate; however, a layer of oxide formed at the NiCrMo coating/substrate interface. Chromium was primarily enriched in the core of splats in the NiCrMo coating exposed to KCl, whereas the Cr-depletion zones were mainly observed around the splats along the entire thickness of the coating. In the NiCrMo-SiO₂ coating, the Cr-depletion zone was mainly observed just beneath the formed corrosion products, verifying sufficient Cr reservoirs in the coating to support the formed scale. No sign of Cl was found within the NiCrMo and NiCrMo-SiO₂ coatings in the absence of KCl confirming that HCl alone was not severe for such coatings; however, adding KCl led to the diffusion of Cl especially in NiCrMo.

The magnified cross-section of the NiCrMo coating exposed to O_2+HCl without KCl at 600 °C after 168 h of exposure is shown in Fig. 9. It was found that the formed oxide was rich in Cr, Ni, and O, mostly attributed to $NiCr_2O_4$ as previously identified in the XRD results. The SEM image revealed formation of voids in the coating. The oxide islands with blocky morphology, which uniformly covered the entire surface of the coating, were also seen. In a longer exposure, these individual islands might reach each other to form a continuous oxide layer on the surface.

The magnified cross-section of NiCrMo exposed to O_2+HCl with KCl is shown in Fig. 10. A porous, non-adherent, and thick corrosion product ($\sim 30\ \mu m$) which was duplex in nature was found to entirely cover the coating surface. As revealed by the EDS elemental mapping, the outer layer consisted of a combination of Ni, K, Cr and Cl (which is supposed to be $NiCr_2O_4$, K_2CrO_4 and KCl [30]) in upper zones, as well as a lower zone comprised of Cr and O as well as Ni found in a porous area. The inner oxide layer (extended towards the coating) was rich in Cr. The formation of such outer corrosion products (attributed to thick Cr_2O_3 layer and K_2CrO_4) resulted in enhanced depletion of Cr at those isolated regions and appearance of voluminous breakaway oxides. The growth of a Cr-rich scale required the selective removal of Cr from the coating and, consequently, resulted in the development of a Cr depletion zone in the subsurface region of the coating. The nature and extent of subsurface depletion are reported to be influenced by the exposure conditions, the resistance of the scale to cracking and spalling, and the resistance of the coating to elemental [30]. Clearly, the greater the extent of subsurface Cr depletion, the less likely it is to help the Cr_2O_3 scale to heal or reform in the event of spallation.

Cl was also found at the interface between the coating and the corrosion products, see Fig. 11. While a small amount of Cl was found in the substrate (point A), a higher content of Cl along with O and Fe identified at the coating/substrate interface (point B) verified formation of a new phase rich in these elements. Point C showed that Cl diffused through the NiCrMo coating towards the substrate most probably through the splat boundaries as the main diffusion paths for the corrosive species [30].

The magnified cross-section of NiCrMo- SiO_2 exposed to O_2+HCl without KCl is shown in Fig. 12. The corrosion product consisted of an outer Si-rich and an inner Cr-rich oxide scale, which uniformly covered the coating surface. A close inspection of the scale formed on the NiCrMo- SiO_2 coating exposed to O_2+HCl with KCl (Fig. 13), showed that it consisted of a non-continuous Si-rich layer at the gas/oxide scale interface, as confirmed by EDS. From the BSE-SEM image in Fig. 13, this Si-rich oxide layer was only about $0.3\ \mu m$ thick. Based on composition and thermodynamic analyses, the Si-rich oxide layer was inferred to be SiO_2 . Such formed SiO_2 scale was not sufficiently protective as O and Cl were found to be present beneath the top SiO_2 layer. The growth of oxide and chloride scales was mainly caused by the inward diffusion of Cl through the oxide leading to the oxide formation, based on the two-step mechanism proposed in a previous work [30]. While the metallic chlorides were formed near the coating/oxide scale interface (lower zones in the formed corrosion product), the oxides were formed at the gas/oxide scale interface (upper zones in the formed corrosion product). The resulting Cr_2O_3 scale

on the NiCrMo-SiO₂ coating was less prone to spallation or void formation compared to NiCrMo after the same exposure time of 168 h. The better adhesion of corrosion products on NiCrMo-SiO₂ might be attributed to the less formation of chlorides at the coating/oxide interface (compared to the SiO₂-free coating). Thus, less vacancies and voids formed at the oxide scale/coating interface, which improved the adhesion of the scale to the substrate. This improved adhesion was qualitatively manifested as a decreased tendency of the scale to spall during the course of exposure and the formation of thinner corrosion product on NiCrMo-SiO₂.

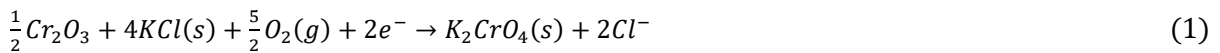
It was already reported that Mo is among the most resistant elements in chlorine-containing atmospheres. It was found that the minor alloying elements such as Mo, present in the coatings can support the formation of protective chromia [49], [50]. Zahs et al. studied [40] the chlorine-induced high temperature corrosion of a wide range of alloys with focus on the behaviour of the alloying elements between 400-700 °C. In all alloy systems Mn, Fe as well as Cr were preferentially attacked while Mo and Ni enriched as leftovers on the surface of the alloys. Thermodynamically, Ni and Mo are rather similar concerning their chlorination reaction [28]. However, the activation energy of the dissociative adsorption of chlorine on the metal surface is also much higher for Mo than for Ni [51]. It was reported that the reaction of Mo and Cl₂ is less thermodynamically favored than the reaction between Cr with Cl₂, because the free energy of Mo-chlorides formation is less than the values for Cr-chlorides formation (~-253 kJ/mol for MoCl₃, ~-350 kJ/mol for CrCl₃, and ~-287 kJ/mol for CrCl₂ at 600 °C). In addition, the amount of chlorine atoms needed for the formation of a stable chloride is higher for Mo because of its higher oxidation numbers in stable chlorides [52]. Due to all of these reasons, the chlorination of Mo is a rather slower reaction than that of Ni or Cr.

3.5 Proposed Cl-induced high temperature corrosion mechanism

Schematics of the corrosion mechanisms taking place in the coatings exposed to HCl-containing environment with and without KCl are shown in Figs. 14, 15 and 16. As can be seen in Fig. 14a showing the corrosion mechanism in the absence of KCl, Cr³⁺ diffuses outward through the grain boundaries of the oxide formed on the NiCrMo coating based on the “electrochemical” mechanism to meet O²⁻ which diffuses inward through the scale [53], [54]. The oxide scale formed on the surface was discontinuous leading to a Cr-depletion zone beneath the oxide scale. However, in NiCrMo-SiO₂ (see Fig. 14b), SiO₂ decelerated short-circuit diffusion of Cr³⁺ through the scale and promoted the selective oxidation of Cr to form the protective Cr-rich oxide scale. Based on the weight change measurement in Fig. 5, the transport through the Cr-rich oxide scale formed on NiCrMo-SiO₂ was manifestly slower than that through the oxide formed on the SiO₂-free coating suggesting that the transport through the latter cannot be a “bulk-diffusion” process. The effect of the dispersoids is then to retard the “short-circuit” diffusion of Cr³⁺ through the oxide defects such as vacancies [25]. The uniform supply of Cr into the continuous oxide scale leads to no subsurface depletion of Cr in the coating. Due to outward diffusion of Cr³⁺, new oxide was formed at the oxide scale/gas interface on the NiCrMo-SiO₂ coating, the vacancies and voids

did not form at the coating/oxide scale interface, so the adhesion of scale-coating was also improved. Such behavior was already seen in a previous work reported by Stringer et al. [24], [25]. It was already shown that the dispersoids on the surface promote development of the first-formed Cr_2O_3 , thus decreasing the internuclear spacing between the Cr_2O_3 nuclei. Such reduction in the internuclear distance leads to a drop in the time required for the lateral growth process to form a complete layer of Cr_2O_3 , and terminates the formation of other transient oxides such as Ni-rich oxides.

Fig. 15 shows a schematic of corrosion mechanism in NiCrMo exposed to KCl. The two-step mechanism was thoroughly explained in a previous work [30]. To summarize the mechanism, in the first step, the corrosion is initiated by the formation of K_2CrO_4 and Cl^- in a reaction between KCl and protective Cr_2O_3 (Eq. 1). K_2CrO_4 depletes the oxide scale in Cr leading to a loss of the protective properties of Cr_2O_3 . The metallic chlorides and Cl_2 form in this stage. In the second step, the formed Cl_2 diffuses inward through the defects (cracks and pores) of the non-protective oxide scale formed in the previous step. Cl^- and Cl_2 diffuse through the oxide grain boundaries (“electrochemical” mechanism [55], [56]) and oxide’s defects (“active-corrosion” mechanism [40], [57]) respectively to reach the coating/oxide scale interface. Vaporization of the metallic chlorides occurs in this step, which leads to formation of the gap at the coating/chloride layer. More detailed information regarding the proposed mechanism and the dominant corrosion reactions can be found in [30].



Adding SiO_2 dispersoids to the NiCrMo coating, Cr^{3+} was continuously supplied to the formed protective Cr_2O_3 scale in step 1, Fig. 16. Therefore, formation of Cl^- and K_2CrO_4 , which depletes Cr_2O_3 in Cr, was slowed down (see Eq. 1 and step 2 in Fig. 16). Consequently, less volatile metallic chlorides and accordingly voids formed in the corrosion products on the coating. Several explanations have been proposed for the lower oxidation rate of the oxide-dispersed alloys [19], [23], [58], [59]. Stringer et al. [25] suggested that the dispersoids (such as ThO_2 , Y_2O_3 , and CeO_2) lying in the surface act as oxide nucleation sites, and led to a faster formation of a continuous Cr_2O_3 scale. Giggins and Pettit [60], using a Pt marker, showed that the position of the markers depends on the relative diffusion rates of the components involved, i.e., outward diffusion of Cr^{3+} and inward diffusion of O^{2-} . They suggested that the slow outward diffusion of Cr^{3+} might be caused by the blocking action of dispersoids (like ThO_2) in the Cr_2O_3 scale. These studies were performed in ambient air (without KCl) and no focus was on the Cl^- and K_2CrO_4 formation on the formed corrosion product. Based on the results obtained in this study, while the SiO_2 -free NiCrMo coating was severely affected by the presence of KCl, the SiO_2 -containing NiCrMo coating showed improved corrosion resistance.

4 Conclusions

The NiCrMo and NiCrMo-SiO₂ coatings were thermally sprayed using the HVAF technique. The high temperature chlorine corrosion behavior of the coatings was studied in 5%O₂ + 500vppm HCl + N₂, with and without KCl addition, to investigate the effect of SiO₂;

1) The effect of SiO₂ was more significant in corrosion protection in harsher corrosive environment once KCl was introduced to the O₂+HCl environment. The difference between the weight change of NiCrMo and NiCrMo-SiO₂ was very low in the absence of KCl, whereas NiCrMo showed much higher weight change than NiCrMo-SiO₂ when KCl was introduced.

2) In the presence of the SiO₂ dispersoids, the selective oxidation of Cr to form a continuous Cr₂O₃ scale was promoted. The adhesion of scale-coating was greatly improved. The uniform supply of Cr to the formed chromia scale promoted the formation of a thin and dense Cr₂O₃ scale that exhibited low growth kinetics and less spallation. Moreover, fast formation of an external Cr₂O₃ scale as a result of the presence of SiO₂ resulted in notably enhanced corrosion resistance of the coating. The non-adherent scale on the SiO₂-free coating underwent fast grain growth.

3) Once KCl was introduced, NiCrMo underwent a two-step corrosion mechanism. In the first step, Cl⁻ diffused through the oxide's grain boundaries based on the electrochemical mechanism, while in the second step, Cl₂ diffused through the oxide's pores. Formation of the volatile metallic chlorides led to the enhanced weight change and deep Cr-depletion zone.

4) Adding SiO₂ dispersoids to NiCrMo, Cr³⁺ was continuously supplied to the formed protective Cr₂O₃ scale. Therefore, formation of Cl⁻ and K₂CrO₄, which depleted Cr₂O₃ in Cr in the first step, was decelerated.

Acknowledgment

Financial support of the Knowledge Foundation for the SCoPe project (RUN 20160201) and Västra Götalandsregionen (VGR) for the PROSAM project (RUN 2016-01489) are highly acknowledged. The authors would like to thank Mr. Jonas Olsson, Mr. Stefan Björklund, and Mr. Kenneth Andersson for their valuable help and advice in processing and characterization of the HVAF coatings in this study. Dr. Mingwen Bai and Mr. Liam Reddy at The University of Nottingham are highly appreciated for the help in running the corrosion exposures.

Reference

- [1] A. Demirbas, "Potential applications of renewable energy sources, biomass combustion problems in boiler power systems and combustion related environmental issues," *Progress in Energy and Combustion Science*, vol. 31, no. 2, pp. 171–192, Jan. 2005.
- [2] A. A. Khan, W. de Jong, P. J. Jansens, and H. Spliethoff, "Biomass combustion in fluidized bed boilers: Potential problems and remedies," *Fuel Processing Technology*, vol. 90, no. 1, pp. 21–50, Jan. 2009.
- [3] H. P. Nielsen, F. J. Frandsen, K. Dam-Johansen, and L. L. Baxter, "Implications of chlorine-associated corrosion on the operation of biomass-fired boilers," *Progress in Energy and Combustion Science*, vol. 26, no. 3, pp. 283–298, 2000.
- [4] D. A. Stewart, P. H. Shipway, and D. G. McCartney, "Influence of heat treatment on the abrasive wear behaviour of HVOF sprayed WC-Co coatings," *Surface and Coatings Technology*, vol. 105, no. 1–2, pp. 13–24, 1998.
- [5] C.-J. Li, G.-J. Yang, and A. Ohmori, "Relationship between particle erosion and lamellar microstructure for plasma-sprayed alumina coatings," *Wear*, vol. 260, no. 11–12, pp. 1166–1172, 2006.

- [6] R. A. Antunes and O. de, "Corrosion in biomass combustion: A materials selection analysis and its interaction with corrosion mechanisms and mitigation strategies," *Corrosion Science*, vol. 76, pp. 6–26, 2013.
- [7] C. Zhang, X. Peng, J. Zhao, and F. Wang, "Hot corrosion of an electrodeposited Ni-11 wt % Cr nanocomposite under molten Na₂SO₄-K₂SO₄-NaCl," *Journal of the Electrochemical Society*, vol. 152, no. 9, pp. B321–B326, 2005.
- [8] M. A. Uusitalo, P. M. J. Vuoristo, and T. A. Mäntylä, "Elevated temperature erosion-corrosion of thermal sprayed coatings in chlorine containing environments," *Wear*, vol. 252, no. 7, pp. 586–594, Apr. 2002.
- [9] S. Matthews, B. James, and M. Hyland, "The role of microstructure in the mechanism of high velocity erosion of Cr₃C₂-NiCr thermal spray coatings: Part 2 — Heat treated coatings," *Surface and Coatings Technology*, vol. 203, no. 8, pp. 1094–1100, Jan. 2009.
- [10] A. Phongphiphat *et al.*, "Investigation into high-temperature corrosion in a large-scale municipal waste-to-energy plant," *Corrosion Science*, vol. 52, no. 12, pp. 3861–3874, Dec. 2010.
- [11] M. Jones, A. J. Horlock, P. H. Shipway, D. G. McCartney, and J. V. Wood, "Microstructure and abrasive wear behavior of FeCr-TiC coatings deposited by HVOF spraying of SHS powders," *Wear*, vol. 249, no. 3–4, pp. 246–253, 2001.
- [12] M. Schütze, M. Malessa, V. Rohr, and T. Weber, "Development of coatings for protection in specific high temperature environments," *Surface and Coatings Technology*, vol. 201, no. 7 SPEC. ISS., pp. 3872–3879, 2006.
- [13] S. Kamal, R. Jayaganthan, S. Prakash, and S. Kumar, "Hot corrosion behavior of detonation gun sprayed Cr₃C₂-NiCr coatings on Ni and Fe-based superalloys in Na₂SO₄-60% V₂O₅ environment at 900 °C," *Journal of Alloys and Compounds*, vol. 463, no. 1–2, pp. 358–372, 2008.
- [14] R. Bhatia, H. Singh, and B. S. Sidhu, "Hot corrosion studies of HVOF-sprayed coating on T-91 boiler tube steel at different operating temperatures," *Journal of Materials Engineering and Performance*, vol. 23, no. 2, pp. 493–505, 2014.
- [15] P. L. Fauchais, J. V. R. Heberlein, and M. I. Boulos, "Industrial Applications of Thermal Spraying Technology," in *Thermal Spray Fundamentals*, Springer US, 2014, pp. 1401–1566.
- [16] M. Rodriguez, M. Staia, L. Gil, F. Arenas, and A. Scagni, "Effect of heat treatment on properties of nickel hard surface alloy deposited by HVOF," *Surface Engineering*, vol. 16, no. 5, pp. 415–420, 2000.
- [17] J. Saaedi, T. W. Coyle, H. Arabi, S. Mirdamadi, and J. Mostaghimi, "Effects of HVOF process parameters on the properties of Ni-Cr coatings," *Journal of Thermal Spray Technology*, vol. 19, no. 3, pp. 521–530, 2010.
- [18] T. S. Sidhu, S. Prakash, and R. D. Agrawal, "Studies on the properties of high-velocity oxy-fuel thermal spray coatings for higher temperature applications," *Mater Sci*, vol. 41, no. 6, pp. 805–823, Nov. 2005.
- [19] K. A. Unocic *et al.*, "High-temperature behavior of oxide dispersion strengthening CoNiCrAlY," *Materials at High Temperatures*, vol. 0, no. 0, pp. 1–12, Nov. 2017.
- [20] P. S. Mohanty, A. D. Roche, R. K. Guduru, and V. Varadaraajan, "Ultrafine particulate dispersed high-temperature coatings by hybrid spray process," *Journal of thermal spray technology*, vol. 19, no. 1–2, pp. 484–494, 2010.
- [21] B. A. Pint, "Study of the Reactive Element Effect in ODS Iron-Base Alumina Formers," *Materials Science Forum*, vol. 251–254, pp. 397–404, 1997.
- [22] D. N. Braski, P. D. Goodell, J. V. Cathcart, and R. H. Kane, "Effect of Y₂O₃ dispersoids in 80Ni-20Cr alloy on the early stages of oxidation at low-oxygen potential," *Oxidation of metals*, vol. 25, no. 1–2, pp. 29–50, 1986.
- [23] T. Huang, J. Bergholz, G. Mauer, R. Vassen, D. Naumenko, and W. J. Quadakkers, "Effect of test atmosphere composition on high-temperature oxidation behaviour of CoNiCrAlY coatings produced from conventional and ODS powders," *Materials at High Temperatures*, vol. 0, no. 0, pp. 1–11, Oct. 2017.
- [24] D. P. Whittle and J. Stringer, "Improvements in high temperature oxidation resistance by additions of reactive elements or oxide dispersions," *Phil. Trans. R. Soc. Lond. A*, vol. 295, no. 1413, pp. 309–329, Feb. 1980.
- [25] J. Stringer, B. A. Wilcox, and R. I. Jaffee, "The high-temperature oxidation of nickel-20 wt. % chromium alloys containing dispersed oxide phases," *Oxid Met*, vol. 5, no. 1, pp. 11–47, Oct. 1972.
- [26] E. Sadeghimeresht, H. Hooshyar, N. Markocsan, S. Joshi, and P. Nylén, "Oxidation Behavior of HVAF-Sprayed NiCoCrAlY Coating in H₂-H₂O Environment," *Oxid Met*, pp. 1–16, Jul. 2016.
- [27] T. Pettersson, "Characterization of Metal Powders Produced by Two Gas Atomizing Methods for Thermal Spraying Applications," KTH Royal Institute of Technology, Stockholm, 2016.
- [28] E. Sadeghimeresht, L. Reddy, T. Hussain, M. Huhtakangas, N. Markocsan, and S. Joshi, "Influence of KCl and HCl on high temperature corrosion of HVAF-sprayed NiCrAlY and NiCrMo coatings," *Materials & Design*, vol. 148, pp. 17–29, Jun. 2018.
- [29] E. Sadeghimeresht, N. Markocsan, and P. Nylén, "A Comparative Study on Ni-Based Coatings Prepared by HVAF, HVOF, and APS Methods for Corrosion Protection Applications," *J Therm Spray Tech*, vol. 25, no. 8, pp. 1604–1616, Dec. 2016.
- [30] E. Sadeghimeresht, L. Reddy, T. Hussain, N. Markocsan, and S. Joshi, "Chlorine-induced high temperature corrosion of HVAF-sprayed Ni-based alumina and chromia forming coatings," *Corrosion Science*, vol. 132, pp. 170–184, Mar. 2018.
- [31] G. Y. Lai, *High-Temperature Corrosion and Materials Applications*. ASM International, 2007.
- [32] C. A. Schneider, W. S. Rasband, and K. W. Eliceiri, "NIH Image to ImageJ: 25 years of image analysis," *Nat Meth*, vol. 9, no. 7, pp. 671–675, Jul. 2012.
- [33] E. Sadeghimeresht, N. Markocsan, P. Nylén, and S. Björklund, "Corrosion performance of bi-layer Ni/Cr₂C₃-NiCr HVAF thermal spray coating," *Applied Surface Science*, vol. 369, pp. 470–481, Apr. 2016.
- [34] E. Sadeghimeresht, N. Markocsan, and S. Joshi, "Isothermal oxidation behavior of HVAF-sprayed Ni and NiCr coatings in H₂-H₂O environment," *Surface and Coatings Technology*, vol. 317, pp. 17–25, May 2017.
- [35] E. Sadeghimeresht, N. Markocsan, and P. Nylén, "A Comparative Study of Corrosion Resistance for HVAF-Sprayed Fe- and Co-Based Coatings," *Coatings*, vol. 6, p. 16, Mar. 2016.

- [36] E. Sadeghimeresht, N. Markocsan, and P. Nylén, "Microstructural and electrochemical characterization of Ni-based bi-layer coatings produced by the HVOF process," *Surface and Coatings Technology*, vol. 304, pp. 606–619, Oct. 2016.
- [37] B. Song, Z. Pala, K. T. Voisey, and T. Hussain, "Gas and liquid-fuelled HVOF spraying of Ni50Cr coating: Microstructure and high temperature oxidation," *Surface and Coatings Technology*, 2016.
- [38] Y. S. Li, Y. Niu, and M. Spiegel, "High temperature interaction of Al/Si-modified Fe–Cr alloys with KCl," *Corrosion Science*, vol. 49, no. 4, pp. 1799–1815, Apr. 2007.
- [39] S. M. Schnurre, J. Gröbner, and R. Schmid-Fetzer, "Thermodynamics and phase stability in the Si–O system," *Journal of Non-Crystalline Solids*, vol. 336, no. 1, pp. 1–25, Apr. 2004.
- [40] A. Zahs, M. Spiegel, and H. J. Grabke, "Chloridation and oxidation of iron, chromium, nickel and their alloys in chloridizing and oxidizing atmospheres at 400–700°C," *Corrosion Science*, vol. 42, no. 6, pp. 1093–1122, 2000.
- [41] M. A. Uusitalo, P. M. J. Vuoristo, and T. A. Mäntylä, "High temperature corrosion of coatings and boiler steels below chlorine-containing salt deposits," *Corrosion Science*, vol. 46, no. 6, pp. 1311–1331, Jun. 2004.
- [42] M. Oksa, S. Tuurna, and T. Varis, "Increased Lifetime for Biomass and Waste to Energy Power Plant Boilers with HVOF Coatings: High Temperature Corrosion Testing Under Chlorine-Containing Molten Salt," *J Therm Spray Tech*, vol. 22, no. 5, pp. 783–796, Jun. 2013.
- [43] N. Israelsson *et al.*, "A Microstructural and Kinetic Investigation of the KCl-Induced Corrosion of an FeCrAl Alloy at 600 °C," *Oxid Met*, vol. 84, no. 1–2, pp. 105–127, Aug. 2015.
- [44] L. Zhu, X. Peng, J. Yan, and F. Wang, "Oxidation of a novel chromium coating with CeO₂ dispersions," *Oxidation of Metals*, vol. 62, no. 5–6, pp. 411–426, 2004.
- [45] P. Platt, V. Allen, M. Fenwick, M. Gass, and M. Preuss, "Observation of the effect of surface roughness on the oxidation of Zircaloy-4," *Corrosion Science*, vol. 98, pp. 1–5, Sep. 2015.
- [46] S. Cruchley, H. E. Evans, M. P. Taylor, M. C. Hardy, and S. Stekovic, "Chromia layer growth on a Ni-based superalloy: Sub-parabolic kinetics and the role of titanium," *Corrosion Science*, vol. 75, no. Supplement C, pp. 58–66, Oct. 2013.
- [47] S. S. Kalsi, T. S. Sidhu, and H. Singh, "Performance of cold spray coatings on Fe-based superalloy in Na₂SO₄–NaCl environment at 900°C," *Surface and Coatings Technology*, vol. 240, pp. 456–463, Feb. 2014.
- [48] J. Pettersson, H. Asteman, J.-E. Svensson, and L.-G. Johansson, "KCl induced corrosion of a 304-type austenitic stainless steel at 600 °C; the role of potassium," *Oxidation of Metals*, vol. 64, no. 1–2, pp. 23–41, 2005.
- [49] D. W. Yun, S. M. Seo, H. W. Jeong, and Y. S. Yoo, "The effects of the minor alloying elements Al, Si and Mn on the cyclic oxidation of Ni–Cr–W–Mo alloys," *Corrosion Science*, vol. Complete, no. 83, pp. 176–188, 2014.
- [50] S. B. S. Kalsi, T. S. Sidhu, and H. Singh, "Performance of cold spray coating in industrial medical waste incinerator," *Surface Engineering*, vol. 30, no. 5, pp. 352–360, Jun. 2014.
- [51] Galetz M.C., Rammer B., and Schütze M., "Refractory metals and nickel in high temperature chlorine-containing environments - thermodynamic prediction of volatile corrosion products and surface reaction mechanisms: a review," *Materials and Corrosion*, vol. 66, no. 11, pp. 1206–1214, Jun. 2015.
- [52] R. Bender and M. Schütze, "The role of alloying elements in commercial alloys for corrosion resistance in oxidizing-chloridizing atmospheres. Part I: Literature evaluation and thermodynamic calculations on phase stabilities," *Materials and Corrosion*, vol. 54, no. 8, pp. 567–586, Aug. 2003.
- [53] J. Pettersson, H. Asteman, J.-E. Svensson, and L.-G. Johansson, "KCl Induced Corrosion of a 304-type Austenitic Stainless Steel at 600°C; The Role of Potassium," *Oxid Met*, vol. 64, no. 1–2, pp. 23–41, Aug. 2005.
- [54] N. Israelsson *et al.*, "A Microstructural and Kinetic Investigation of the KCl-Induced Corrosion of an FeCrAl Alloy at 600 °C," *Oxid Met*, vol. 84, no. 1–2, pp. 105–127, Aug. 2015.
- [55] S. Kiamehr, K. V. Dahl, M. Montgomery, and M. a. J. Somers, "KCl-induced high temperature corrosion of selected commercial alloys," *Materials and Corrosion*, vol. 66, no. 12, pp. 1414–1429, Dec. 2015.
- [56] J. Pettersson, C. Pettersson, H. Asteman, J.-E. Svensson, and L.-G. Johansson, "A pilot plant study of the effect of alkali salts on initial stages of the high temperature corrosion of alloy 304L," *Materials Science Forum*, vol. 461–464, no. II, pp. 965–972, 2004.
- [57] H. J. Grabke, E. Reese, and M. Spiegel, "The effects of chlorides, hydrogen chloride, and sulfur dioxide in the oxidation of steels below deposits," *Corrosion Science*, vol. 37, no. 7, pp. 1023–1043, Jul. 1995.
- [58] G. Hou, Y. An, X. Zhao, H. Zhou, and J. Chen, "Effect of alumina dispersion on oxidation behavior as well as friction and wear behavior of HVOF-sprayed CoCrAlYTaCSi coating at elevated temperature up to 1000°C," *Acta Materialia*, vol. 95, no. Supplement C, pp. 164–175, Aug. 2015.
- [59] K. Arnold, G. Tatlock, C. Kenel, A. Colella, and P. Matteazzi, "High temperature isothermal oxidation behaviour of an Oxide dispersion strengthened derivative of IN625," *Materials at High Temperatures*, vol. 0, no. 0, pp. 1–10, Oct. 2017.
- [60] C. S. Giggins and F. S. Pettit, "The oxidation of TD NiC (Ni-20Cr-2 vol pct ThO₂) between 900° and 1200°C," *MT*, vol. 2, no. 4, pp. 1071–1078, Apr. 1971.

Captions of Figures

Fig. 1. SEM topographic (SE mode) and cross-section (BSE mode) of; a, b) NiCrMo and c, d) NiCrMo-SiO₂ powders, and the corresponding EDS analysis.

Fig. 2. Topographical SEM micrographs (SE mode) of the as-sprayed a) NiCrMo, and b) NiCrMo-SiO₂ coatings.

Fig. 3. SEM micrographs (BSE mode) of cross-sections of the polished coatings, coating/substrate interfaces, and EDS point analysis, a) NiCrMo, and b) NiCrMo-SiO₂.

Fig. 4. XRD patterns of the feedstock powders and corresponding polished NiCrMo and NiCrMo-SiO₂ coatings.

Fig. 5. a) weight change of the exposed NiCrMo and NiCrMo-SiO₂ coatings in 5% O₂ + 500 ppm HCl + N₂ with and without KCl deposit for up to 168 h at 600 °C, and b) squared of weight gain versus time (sec.). k_p value for NiCrMo exposed to KCl was measured within the exposure period from 0 to 96 h to avoid the interference by the weight change drop observed from 96 to 168 h.

Fig. 6. XRD patterns of the exposed NiCrMo and NiCrMo-SiO₂ coatings in 5% O₂ + 500 ppm HCl + N₂ with and without KCl deposit up to 168 h at 600 °C.

Fig. 7. SEM topographic micrographs (SE mode) of the coatings exposed in 5% O₂ + 500 ppm HCl + N₂ with KCl for 168 h at 600 °C a) NiCrMo and, b) NiCrMo-SiO₂.

Fig. 8. Back-scattered SEM micrographs of cross-sections of the exposed coating in 5% O₂ + 500 ppm HCl + N₂ for 168 h at 600 °C, a) NiCrMo exposed without KCl, b) NiCrMo exposed with KCl, c) NiCrMo-SiO₂ exposed without KCl, and d) NiCrMo-SiO₂ exposed with KCl.

Fig. 9. Back-scattered SEM micrographs of cross-sections of the exposed NiCrMo coating in 5% O₂ + 500 ppm HCl + N₂ without KCl deposit for 168 h at 600 °C.

Fig. 10. Back-scattered SEM micrographs of cross-sections of the exposed NiCrMo coating in 5% O₂ + 500 ppm HCl + N₂ with KCl deposit for 168 h at 600 °C.

Fig. 11. Back-scattered SEM micrograph of the NiCrMo coating/substrate exposed in 5% O₂ + 500 ppm HCl + N₂ with KCl deposit for 168 h at 600 °C, and the corresponding EDS analysis, point A at the substrate, point B at the coating/substrate interface and point C at the coating.

Fig. 12. Back-scattered SEM micrographs of cross-sections of the exposed NiCrMo-SiO₂ coating in 5% O₂ + 500 ppm HCl + N₂ without KCl deposit for 168 h at 600 °C.

Fig. 13. Back-scattered SEM micrographs of cross-sections of the exposed NiCrMo-SiO₂ coating in 5% O₂ + 500 ppm HCl + N₂ with KCl deposit for 168 h at 600 °C.

Fig. 14. Schematic of corrosion mechanism in the coatings exposed into 5% O₂ + 500 ppm HCl + N₂ for 168 h at 600 °C without KCl deposit, a) NiCrMo, and b) NiCrMo-SiO₂. SiO₂ promoted the selective oxidation of Cr to form the protective Cr-rich oxide scale on NiCrMo-SiO₂. While a (Cr,Ni)-rich oxide formed on NiCrMo, a dense Cr-rich scale formed on NiCrMo-SiO₂.

Fig. 15. Schematic of corrosion mechanism in the NiCrMo coating exposed into 5% O₂ + 500 ppm HCl + N₂ with KCl deposit for 168 h at 600 °C. At the early stages, the corrosion is initiated by the formation of K₂CrO₄ and Cl⁻. K₂CrO₄ depletes the oxide scale in Cr leading to a loss of the protective properties of Cr₂O₃. The metallic chlorides and Cl₂ form in this stage. In the second step, the formed Cl₂ diffuses inward through the defects (cracks and pores) of the non-protective oxide scale formed in the previous step. Cl⁻ and Cl₂ diffuse through the oxide grain boundaries (“electrochemical” mechanism) and oxide’s defects (“active-corrosion” mechanism) respectively to reach the coating/oxide scale interface. Vaporization of the metallic chlorides occurs in this step, which leads to formation of the gap at the coating/chloride layer [45].

Fig. 16. Schematic of corrosion mechanism in the NiCrMo-SiO₂ coating exposed into 5% O₂ + 500 ppm HCl + N₂ with KCl deposit for 168 h at 600 °C. The dispersoids decelerated formation of Cl⁻ and K₂CrO₄ at the early stages. Random diffusion of Cl⁻ within the oxide layer and a few Cr-depleted regions within the coating were observed; however, in general, the dispersoids succeeded to protect the coating and accordingly the substrate by promoting formation of a dense and protective Cr-rich oxide scale.